An Investigation of Integrated Multiscale Three-Dimensional Printing for Hierarchical Structures Fabrication

Xiangjia Li[1]
Department of Aerospace and Mechanical Engineering,
School for Engineering of Matter, Transport and Energy,
Arizona State University,
501 E. Tyler Mall,
Tempe, AZ 85287
e-mail: xiangjia.li@asu.edu

Tommaso Baldacchini
Department of Chemistry,
University of California Irvine,
Irvine, CA 92697
e-mail: tbaldacchini@gmail.com

Yong Chen[1]
Department of Aerospace and Mechanical Engineering,
Epstein Department of Industrial and Systems Engineering,
University of Southern California,
3715 McClintock Ave.,
Los Angeles, CA 90089-01932
e-mail: yongchen@usc.edu

Nature provides us with a large number of functional material systems consisting of hierarchical structures, where significant variations in dimensions are present. Such hierarchical structures are difficult to build by traditional manufacturing processes due to manufacturing limitations. Nowadays, three-dimensional (3D) objects with complex structures can be built by gradually accumulating in a layer-based additive manufacturing (AM); however, the hierarchical structure measured from macroscale to nanoscale sizes still raises significant challenges to the AM processes, whose manufacturing capability is intrinsically specified within a certain scope. It is desired to develop a multiscale AM process to narrow this gap between scales of feature in hierarchical structures. This research aims to investigate an integration approach to fabricating hierarchical objects that have macro-, micro-, and nano-scales features in an object. Firstly, the process setup and the integrated process of two-photon polymerization (TPP), immersed surface accumulation (ISA), and mask image projection-based stereolithography (MIP-SL) were introduced to address the multiscale fabrication challenge. Then, special hierarchical design and process planning toward integrating multiple printing processes are demonstrated. Lastly, we present two test cases built by our hierarchical printing method to validate the feasibility and efficiency of the proposed multiscale hierarchical printing approach. The results demonstrated the capability of the developed multiscale 3D printing process and showed its future potential in various novel applications, such as optics, microfluidics, cell culture, as well as interface technology. [DOI: 10.1115/1.4054317]

Keywords: multiscale, additive manufacturing, bioinspiration, photopolymerization, hierarchical fabrication

Introduction

Many material systems in nature exhibit outstanding properties not found in artificial systems. The exceptional performance of natural materials, such as the structural color of butterfly, the drag force reduction of fish scales, the superhydrophobic effect of Salvinia Paradox, and water collection of desert beetles, benefit from hierarchical structures over a large range of scales from macroscale to nanoscale [1,2]. Such multiscale structures in nature inspire composite material design and show promising multifunctional applications in mechanical, optical, thermal, and electrical fields [2–4]. Meanwhile, structures found in nature possess comprehensive complexity in geometry, hierarchy, and material, setting challenges over the fabrication of such structures with traditional manufacturing approaches. Additive manufacturing (AM), as a solution, can fabricate objects with complex shapes by depositing material layer by layer [5,6]. Due to such unique fabrication capability, recent advances in AM technology have shown progressive achievements in a wide variety of areas, including the fabrication of bio-inspired structures and materials [7,8]. However, most AM technologies have the capability of fabricating three-dimensional (3D) structures at a single scale. For example, selective laser sintering/melting (SLS/M) is used to fabricate objects with the geometric features at the macro- or meso- scale using metal, ceramic and plastic powders [9]. Similarly, fused deposition modeling (FDM) is developed to build mesoscale objects by the extrusion of constant filament [9]. Besides, both inkjet printing and polyjet printing are used to fabricate objects with features limited to microscale using polymer or hydrogel [9].

Recently, a few 3D printing approaches were developed in an attempt to achieve manufacturing at multiple scales [10]. For example, the multiscale biomimetic blood vessel was printed by injecting biocompatible material into revisable gel through a microscale nozzle head [11–13]. Biomimic multiscale shark skin was designed and fabricated to achieve high hydrodynamic performance, using a microscale laser-based printing process [14]. To increase the fabrication resolution and efficiency of the laser-based stereolithography process, Mao, etc. Proposed an optimized multiscale printing process by integrating multidimensional shaped laser beam and selecting the laser beam with appropriate dimensions based on the fabrication requirements [15]. Also, Zhou et al. Proposed a stereolithography (SL) based multiscale manufacturing approach by integrating hybrid light sources including laser and digital projection light [16]. Similarly, a hybrid-light-source SL process was developed to fabricate macroscale objects with microscale textures [17]. Besides, advanced multimaterials devices in micro-and nanoscales can be printed by electrohydrodynamic printing, although the fabrication time will be significantly longer due to the printing principle [18].

Overall, most of the current AM fabrication procedures for the printing of multiscale hierarchical structures are associated with experimental complexity and limited flexibility, especially when the desired object has an overall dimension at the macroscale level yet with micro- and nanoscales features in detail. Therefore, the development of multiscale AM processes with the fabrication capability ranging from macroscale to nanoscale is highly valuable and necessary for the fabrication of bio-inspired devices for functional applications in different engineering fields. In general, each type of AM process is considered to have its most

[1]Corresponding authors.

Contributed by the Manufacturing Engineering Division of ASME for publication in the Journal of Micro- and Nano-Manufacturing. Manuscript received December 25, 2021; final manuscript received April 6, 2022; published online April 27, 2022. Assoc. Editor: TieJun Zhang.

appropriate printing scope, in which the optimized resolution is determined by its intrinsic printing principle. For example, the overall dimensions of the structures in macroscale fabrication are from centimeters to millimeters with feature sizes of the order of 1000 s of microns, and the smallest feature size is hundreds of microns. While the fabrication dimension of the microscale process is 10 times smaller than the one in macroscale fabrication, and the resolution of the microscale process can be tens of microns. In nanoscale fabrication, the printing capability is from hundreds of microns to submicron. It is desired to fabricate features at different scales using the 3D printing processes whose scope best suits the purposive fabrication [19–21]. For example, based on the natural architecture of *gecko*'s feet where macro, meso, micro, and nanofeatures are presented [22], the fabrication process of the design should be synchronized as the features scale down, in a hierarchical manner that macro- and meso- structures being built by the macrolevel process, followed by the fabrication of micro-and nanoscale features through each of their scale-matching processes (Fig. 1(*a*)).

The idea of integrating several scale-exclusive 3D printing methods is intuitive; however, it has put forward two major demands for the process development: first is to allocate each subprocess at the best of their advantages, and second is to investigate how to integrate these processes seamlessly. Based on our previous work, the mask image projection-based stereolithography (MIP-SL) process is highly efficient in building objects with features that are at macro- and meso- scales [23–29]. In MIP-SL, the illuminated light is reflected by the Digital Micromirrors Device (DMD), where the light intensity can be changed based on the angle of the micromirror in the DMD [23]. After going through optical lenses, the focusing image irradiates at the resin surface; accordingly, the resin will be cured after a suitable exposure to light (Fig. 1(*b*)). Since the DMD has millions of mirrors and each mirror represents one pixel in the focusing image, the projected mask image can achieve high-resolution light exposure [23]. Using different optical lenses designs, the mask images can achieve different projection sizes, ranging from several millimeters to several hundreds of millimeters [23–27]. Based on optimized pixel blending, the accuracy and surface finish of macroscale features printed by MIP-SL were improved dramatically [23,24]. A macroscale part with mesoscale features can be printed within minutes instead of hours that are typically required by using either two-way movements or mask video projection [25,26]. Besides, different types of materials including hydrogel, nanocomposite, and polymer, can be fabricated to construct a solid object with desired material distributions using MIP-SLA [29–31]. Compared with other 3D printing processes, the MIP-SL process is highly efficient in building objects with features that are in macro- and meso- scales, since each layer of material can be cured by one-time exposure using a high resolution two-dimensional (2D) light beam [23–25]. However, when dealing with microscale and even submicron features, the MIP-SL shows its drawbacks. The fabricated features tend to be less sharp due to the limited pixel resolution and the light accumulation effect among adjacent pixels that may distort the desired shape [28]. Considering the above pros and cons, we have selected MIP-SL as a suitable candidate for the fabrication of macroscale and meso-scale features [23–27].

In terms of nanofabrication, two photon polymerization (TPP) is one type of maskless lithography that enables the fabrication of submicron structures with features smaller than 100 nm using photocurable polymer [32–36]. Since the TPP was developed based on the laser writing process, and the photosensitive material is not accumulated in a layer-based manner, there are no topological constraints of geometrical shape that can be printed by TPP [33,34]. Moreover, the crosslink of photocurable polymer is caused by the nonlinear optical light absorption of multiple photons in TPP, hence TPP is capable of fabricating microscale and nanoscale structures with sharp features, which is impossible to be fabricated by using most AM approaches [34]. Due to its special fabrication capability, TPP is extensively used in the fabrication of 3D micro-and nanoscales structures. However, TPP is not ideal

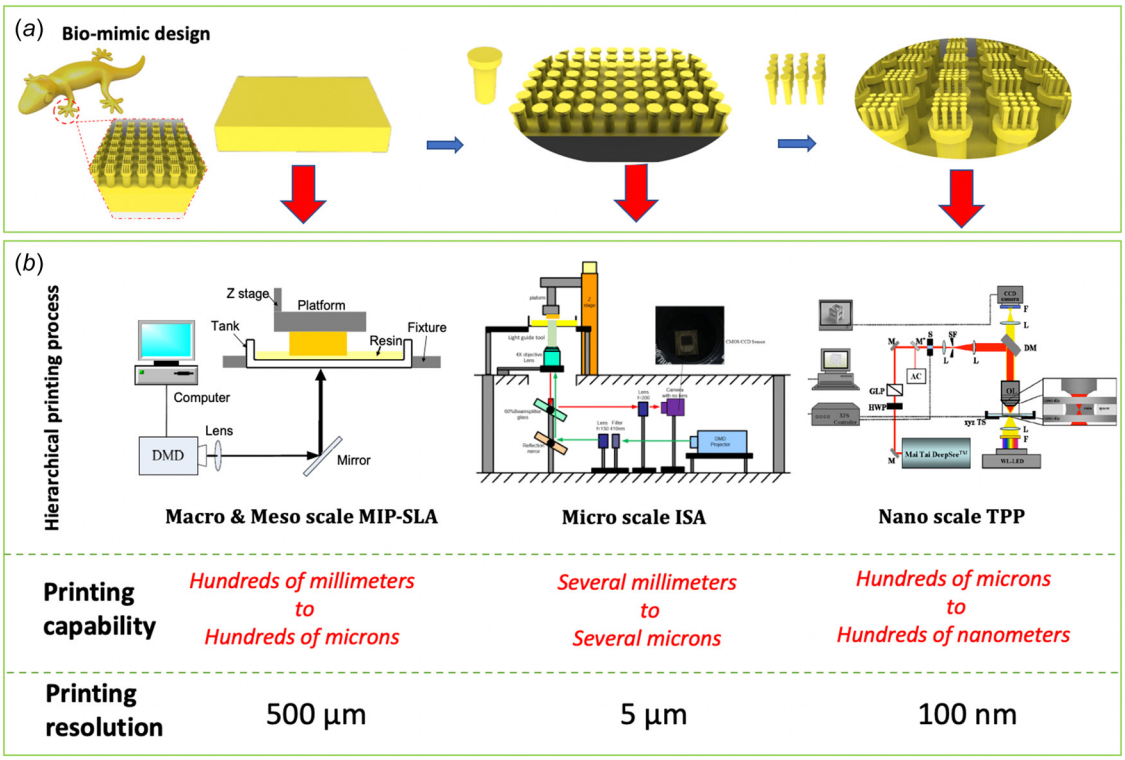

Fig. 1 An illustration of hierarchical structure design and process planning of multiscale 3D printing: (*a*) biomimetic hierarchical structures and (*b*) proposed hierarchical 3D printing process by integrating MIP-SL, ISA, and TPP

for building macro- and meso- scales structures, since there are several challenges when using TPP in making structures on such large scales. First, it is very time-consuming to fabricate macro- and meso- scales structures by TPP with the nanoscale size laser beam, since the laser beam needs to scan the entire volume to construct the 3D object. It took a couple of hours to fabricate 2 mm mesh-shaped structures with a thickness of 500 μm, which only cost 5 min to fabricate by using other microscale printing approaches [37]. Second, the flatness of the object is a critical factor in the TPP process during the fabrication process. Because the laser beam should be focused at the same horizontal position, the macro- and meso- scales fabrication increases the difficulty of the perfect flatness of the printed object [37]. Finally, material cracking may happen due to the shrinkage of the material during/after fabrication [36]. Considering the strength and drawbacks, TPP is an appropriate method to fabricate nanoscale features at high resolution and accuracy [30–34].

To fabricate geometric features in macro-, micro-, and nanoscales, a critical bridge that can connect MIP-SL with TPP is necessary to integrate. Immersed surface accumulation (ISA) process is developed to build microscale features on the surface of preexisting macro- and meso- scales objects [37–39]. Due to the unique light guide tool, the ISA process shows flexibility in building microscale features with complex geometric shapes on the surface of a large-scale object, and both inside and outside surfaces can be decorated with desired microscale structures [37]. The above key features enable ISA to be a promising microscale solution to integrate with MIP-SL and TPP processes for the fabrication of multiscale structures. Hence, in the present research work, we investigated a 3D hierarchical printing approach with a focus on integrating the MIP-SL and TPP processes with the ISA process, for the fabrication of an object with multiscale structures with a dimensional span ranging from macroscale to nanoscale (Fig. 1). To achieve the multiscale fabrication, we design the hardware for integration, developed the vision-assisted alignment for integration, identified the design strategy for the transition between multiple processes, investigated the material fabrication, and conducted process planning capability for multiscale fabrication. Based on our proposed hierarchical printing approach, we demonstrated the potential applications in the fabrication of the multiscale biocompatible scaffold and the bio-inspired optical filter. Furthermore, considering the efficient fabrication strategy of our method, the proposed hierarchical printing is potentially useful in the future development of biomimetic functional devices with multiscale hierarchical structures [2,7].

Process Setup and Integration

In order to integrate three different printing process, a key problem is how to build new features on the prefabricated objects from other processes. For a macroscale object by MIP-SL, both ISA and TPP processes have the flexibility of building around inserts so that microscale and nanoscale features can be deposited on the object. Another key problem to be addressed is how to avoid possible misalignment issues between different AM processes. Accordingly, we added a vision system in both ISA and TPP processes to closely monitor the fabrication process and to provide the alignment of structures that are fabricated on different scales. In the following section, the hardware design and implantation of vision-assisted alignment for the integration of the MIP-SL, ISA, and TPP processes will be discussed in detail.

Hardware Design for Integration of Mask Image Projection-Based Stereolithography and Immersed Surface Accumulation. The ISA process with a bottom-up frame was developed to fabricate 3D microscale structures with an emphasis on building around insert [37]. In ISA, a light guide tool with the DMD-based imaging system was used as the accumulation tool, which was immersed inside the liquid resin to build microscale features on a prefabricated object by continuously projecting the 2D patterned light beam from bottom. To generate the 2D patterned light beam, the ultraviolet (UV) light reflected by the DMD chip went through the collimating lens and finally focused on the end surface of the light guide tool by the 4x objective lens. Since the DMD chip with millions of micromirrors can generate complex and diverse 2D patterned light beams, ISA has the capability of fabricating microscale structures with complex geometric shapes [37,38]. In order to integrate ISA with MIP-SL, in situ visualization module was designed to detect the MIP-SL built object and determine the relative location of the light beam with respect to the MIP-SL built geometry (Fig. 2(*a*)). The in situ vision system contained a beam splitter, a focusing convex lens, and a complementary metal-oxide-semiconductor (CMOS) camera (Fig. 2(*a*)). The light beam illuminating the prebuilt object traveled back through the objective lens and beam-splitter and was focused by a convex lens. To observe the image of the MIP-SL built object and the focused light beam, a CMOS camera was setup behind the focusing convex lens, such that the focused light can be captured by the CMOS camera, and a clear image of the fabrication region was obtained. The size of the view field of CMOS camera is 10 mm x 10 mm and the resolution of the image is 1280 × 720. Besides, the light-emitting diode (LED) emits visible light to illuminate the previously MIP-SL built part (Fig. 2(*a*)). The captured detection image was displayed on a computer monitor with 50× magnifications. Since the light should be able to penetrate through the prebuilt part where the nanoscale features will be printed using TPP process, a glass slide instead of an aluminum block was used as the platform, on which the part was printed using MIP-SL, ISA, and TPP. A pair of magnetic fixed blocks were used to mount the glass slide in both MIP-SL and ISA, which facilitates the transition between multiple processes.

Hardware Design for Integration of Immersed Surface Accumulation and Two-Photon Polymerization. The experimental setup of TPP with top-down frame is shown in Fig. 2(*b*). In TPP, the near-infrared light is applied to trigger the photopolymerization of the liquid resin, where the phase of photosensitive polymer is changed from liquid to solid [34]. To achieve multiphoton absorption, ultrashort and fast pulsed laser and high numerical aperture lenses are used in TPP. The polymerization of photosensitive resin is only excited by the absorption of two or more photons, and the photopolymerization of polymer only occurs at the place where the light intensity of the laser beam reaches the critical value, which is determined by the photosensitivity of the resin [34]. Compared with single-photon absorption, like MIP-SL or ISA, TPP requires much higher energy to solidify the material [34]. The exposure dose of the focused laser beam, which is proportional to the square of the laser intensity, can be modulated by controlling the power of the laser beam, and this nonlinear light intensity modulation allows the fabrication of 3D features that are smaller than the wavelength of light [34]. The dimension of the laser beam, of which the wavelength is 800 nm, can be controlled as small as 100 nm to fabricate nanoscale features [34]. To integrate the ISA and TPP, we developed an in situ monitoring module including a beam splitter, a focusing convex lens, visible LED, collimating lens, charge-coupled device (CCD) monochrome microscope camera. The fabrication area was illumined by the collimated visible light emitted from LED, and the illumination light didn't initiate the photopolymerization of material which only be activated after the absorption of two photons under the exposure of 780 nm laser. The light from the fabrication area will be reflected by the beam splitter and focused on the CCD camera with the resolution of 1920 x 1080. Using the designed in situ monitoring module and the accordingly obtained image, the relative location of the prebuild object and fabrication plane can be determined. Besides, the whole fabrication process can be monitored to improve the printing quality.

Vision-Assisted Alignment. When multiple processes were being integrated, it was necessary to determine the relative

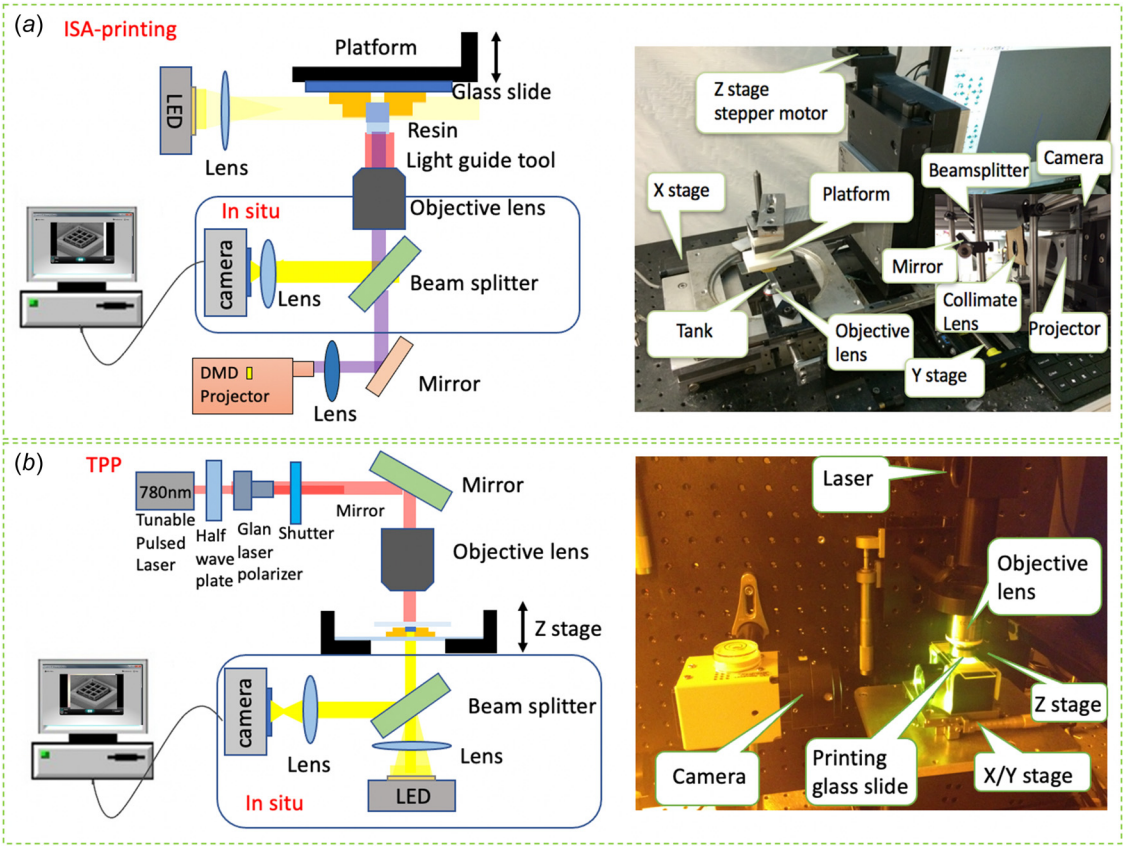

Fig. 2 Hardware design of in situ visualization module in (*a*) ISA and (*b*) TPP for the integration of MIP-SL, ISA, and TPP

location of the light beam to the previously built geometry. To address the issue, optical vision assisted in situ modules were designed and added to both microscale ISA and nanoscale TPP prototype machines, allowing one to observe the location of the curing light and the prebuilt object for the alignment. In terms of the initial position in X/Y plane, assume the center portion of the light beam (1920×1080) was used to build microfeatures. The movements of the stage in the X/Y directions were required for the alignment of the light beam and the prebuilt object. The X and Y stages moved both the tank and the prebuilt object in the corresponding direction. The target of the alignment of different processes was to get the relative position of the curing light and the prebuilt object. With the hardware designs of in situ visualization modules in ISA and YPP, the vision-assisted alignment coordinating the prebuilt objects with different projection lights is used to integrate multiple processes, as presented in Fig. 3(*b*).

In microscale ISA and nanoscale TPP, the illustrative diagram of the relative location between the prebuilt object and the projection light is shown in Fig. 2. To calibrate the camera, a checkerboard was placed on the printing platform and the image of the fabrication area was taken as shown in Fig. 3(*b*). The physical dimension of one pixel in the taken image was determined. After taking an image of the fabrication region with the calibrated projection light beam (Fig. 3(*b*)), the coordinates of four corners $P_0 \sim P_3$ of the calibrated projection light beam were calculated by the captured image, and similarly, the coordinates of four corners $M_0 \sim M_3$ of the prebuilt object also were calculated by taking another image without the calibrated projection light beam. Based on the actual dimensions of the calibrated projection light beam in the X and Y directions, denoted by P_x and P_y, respectively, the real dimension of the pixel in the captured image was further calculated. Then the relative position of the prebuilt part $M_0 \sim M_3$ and the projection light beam $P_0 \sim P_3$ were identified. The coordinates $C_0 \sim C_3$ of four corners of the region, where the new feature would be printed, were set in the coordinate system of the prebuilt object. The projection light beam was located at the relevant processing fabrication area by adjusting the X and Y stages with the calculated distance. The corresponding movement distances X' and Y' of the platform in the X and Y directions were shown in the below equation, respectively

$$\begin{cases} X' = \dfrac{C_{0x} + C_{1x}}{2} + \left(M_{0x} - \dfrac{P_{0x} + P_{1x}}{2} \right) \dfrac{P_x}{P_{1x} - P_{0x}} \\ Y' = \dfrac{C_{0y} + C_{1y}}{2} + \left(M_{0y} - \dfrac{P_{0y} + P_{3y}}{2} \right) \dfrac{P_y}{P_{3y} - P_{0y}} \end{cases} \tag{1}$$

The specific alignment process has the following steps.

- Step 1: project a full-size rectangular light beam. Then mark four corners $P_0 \sim P_3$ of this projection image in the alignment imaging system, and calculate the resolution of each pixel of the captured image in the alignment imaging system based on the real size of the light beam.
- Step 2: mount the pre-built object and move the X and Y stages to allow four corners of the pre-built object to be captured inside the alignment imaging system. Mark four corners $M_0 \sim M_4$ of the pre-built object in the alignment imaging system.
- Step 3: move the X and Y stages with corresponding distances X' and Y' that were calculated based on Eq. 1 to make the center point C of the fabrication region closer to the center point P of the projection image.
- Step 4: Repeat above process to reduce the alignment error. Before the printing process, project the fabrication light beam on the fabrication region of prebuilt object, where the printed feature with smaller scale will be attached to, and

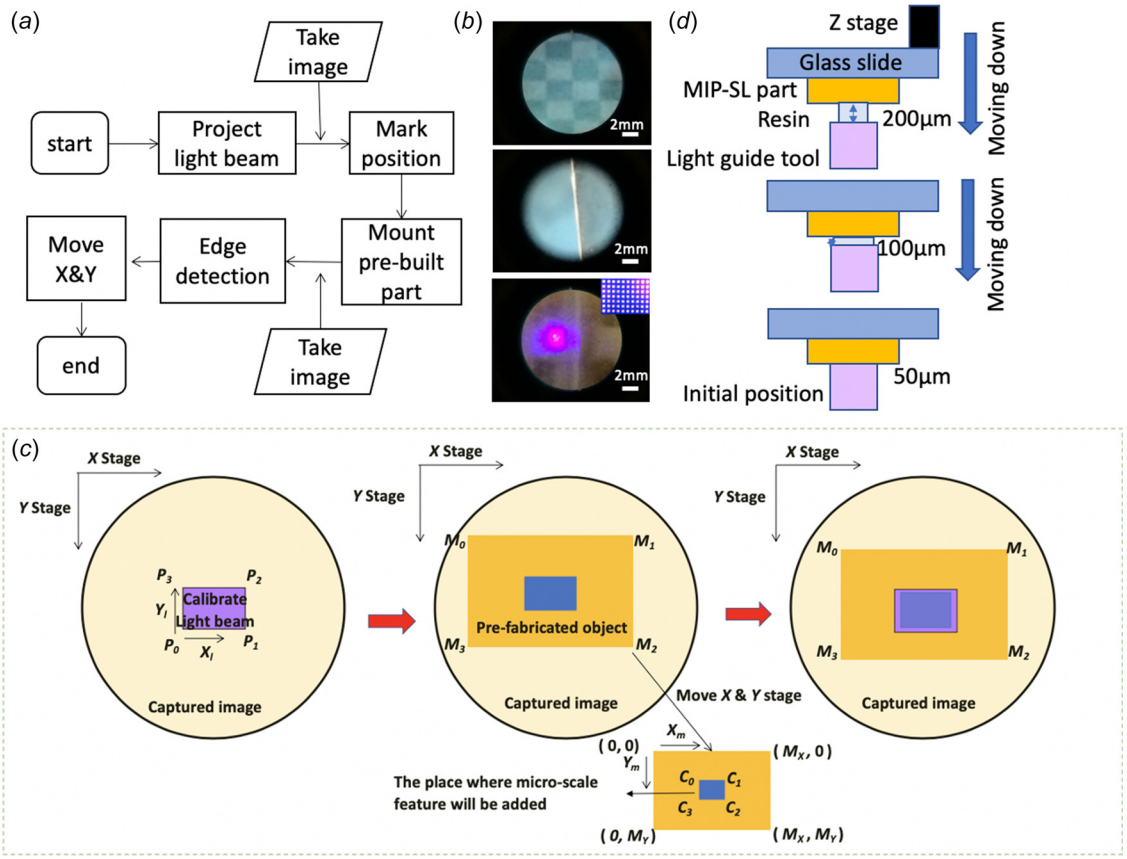

Fig. 3 A vision-assisted alignment module in the integration of MIP-SL, ISA, and TPP: (*a*) flowchart of the vision-assisted alignment module in the microscale ISA and the nanoscale TPP, (*b*) the images taken by the vision-assisted alignment module in the microscale ISA, (*c*) the initial position identification in *X/Y* plane in the microscale ISA process, and (*d*) the initial position identification in *Z* axis in the microscale ISA process

capture the image to further improve the alignment precision.

After calibrating the relevant position of projection beam and prebuilt object in X/Y plane, the photocurable resin was added to the printing area and the relative position of the light guide tool and the prebuilt object in the printing direction was determined by the color level of resin in the captured image in ISA (Fig. 3(*c*)) [37]. Based on the captured images and the platform mounted with the glass slide with prebuilt object was moved to the initial position in the *Z* direction for the fabrication of microscale structures [27]. Similarly, TPP system had a vision-assisted alignment process to observe the prebuilt microscale object. Before the fabrication of submicron features on the prebuilt object, the calibration of the relative position between the focused printing laser and prebuilt object in the TPP process was the same as the aforementioned calibration process between the macroscale MIP-SL and the microscale ISA. By adjusting the position of the glass slide in the *Z* direction using Z linear actuator, the fabrication region, where the submicron features were to be printed, was focused with the help of the vision-assisted system. At the same time, the printing laser was focused on the same *X*/*Y* plane, so that the two-photon cured features were attached on the surface of the prebuilt microscale object. Based on the developed vision-assisted system, the MIP-SL, ISA, and TPP setups can be seamlessly integrated to fabricate various multiscale hierarchical structures ranging from macroscale to nanoscale.

Process Planning and Design of Structures

Transition Region Design and Optimization. During the transition between consecutive processes, e.g., fabricating subsequent features at the same layer of the prebuilt object, the attachment between different scales of features at the transition region is a critical challenge. Particularly, for the overhanging feature with no solid support from the structure built by the previous larger scale AM process, the newly cured feature only attaches to the sidewall of the prebuilt structure with a limited adherence. Without any support structures from the bottom layer of the prebuilt object, the newly cured feature maintains its shape by the bending strength at the endpoint of each side. The bending force of these features is minor due to the limited contact area A and the tensile stress of the material σ_τ so that the deformation caused by the material self-gravity load results in the damage of microscale structure when the new features are written on it. To solve the problem, the area under the overhanging feature should first be printed with a certain amount of transparent polymer that may reinforce underneath for the microscale features to attach (Fig. 4). Compared with original contact area A, the deformation will be largely eliminated with straight support from the layer of material underneath, and the micro-and nanoscales features can be further built on the top surface of the transparent polymer (Fig. 4(*b*)).

Due to the requirement of light penetration for the subsequent process, the material used for building the support should be transparent. Besides, the material used for building micro-and nanostructures on top of the support needs to be transparent to both visible and near-infrared photons. This is because the TPP process in this experiment used an up-right system, where transmission light microscopy was employed to identify predetermined locations (Fig. 4(*a*)). The light penetrable photocurable polymers, such as PEGDA and E-glass, were therefore chosen to fabricate the support to enable the micro/nanostructures to be fabricated on top of the macroscale object. The transparency of material is also critical in helping the alignment process of the fabrication region

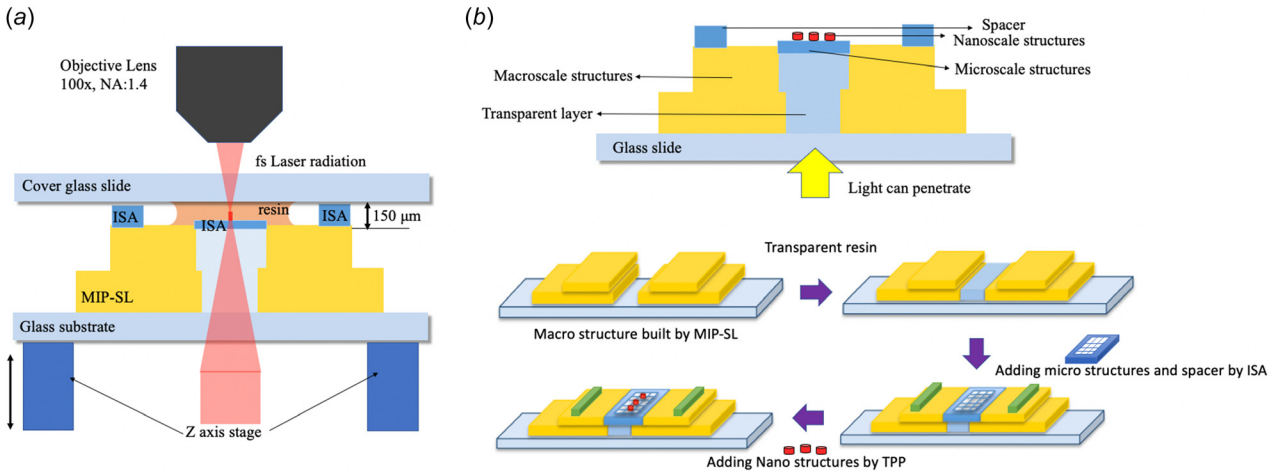

Fig. 4 The transition design between multiple processes: (*a*) an illustration of the transition structure design for the integration of multiple processes and (*b*) the printing procedures of multiscale structures with the transition design

in the integration of two different processes. Meanwhile, a fabrication glass slide was used as the building platform in the integrated MIP-SL, ISA, and TPP processes for its easy transition and superior transparency. We first cured layers of transparent material at the thickness of 500 μm in total as the base that can prevent thin layers of cured polymer from slipping off the smooth surface of the glass slide. Furthermore, the microscale spacers with a height of 150 μm were designed on the multiscale structures and further printed using the microscale ISA process so that the printing resin doesn't need to cover the whole prebuilt object in nanoscale TPP printing system, which avoid significant material waste. With the help of ISA printed microspacers, the liquid bridge of resin was generated between the cover glass slide and the fabrication area of the prebuild object, providing enough resin for the fabrication of nanoscale features (Fig. 4(*a*)). Besides, the spacers provide a potential feeler gauge and help in positioning the focused laser spot on the fabrication area of prebuilt object in Z direction.

Material Curing Performance Optimization. In the photopolymerization-based MIP-SL and ISA processes, the photocurable polymer is accumulated into 3D structures layer-by-layer after the initiation by the absorption of UV light. The vertical printing resolutions of MIP-SL and ISA processes are determined by the depth that light can penetrate in the photopolymerizable medium. To construct a multiscale 3D object using the proposed integrated process, the penetration of the projected light beam should be sufficiently deep to ensure the newly cured layer can be attached to the surface of the prebuilt object. However, if the light penetrates de-eply in the photocurable resin medium, it may not only solidify the next layer of the object at the surface but also results in unexpected polymerizations in previously polymerized layers of prebuilt object [40]. The cure depth of photopolymer C_d is used to quantitatively represent the degree of the difficulty of light penetration [41]. In microscale fabrication, e.g., ISA, where the layer thickness only spans from 10 μm to 50 μm. Due to the microlevel geometry, the material with a high range of light penetration is prone to have over cure at the built regions. Also, the cure depth is sensitive to alter as it changes dramatically with the modification of the exposure time [42]. Therefore, the material curing performance of photocurable polymer should be studied in order to achieve integration of microscale ISA and macroscale MIP-SL. For the printing process of the microscale ISA and macroscale MIP-SL system, the layer thickness usually was 10–50 μm and 75–150 μm, respectively [24,37]. In consideration of solid attachment between the adjacent layers and the surface quality of the 3D printed part, the layer thickness is set to be half of the cure depth of the material in the macroscale fabrication [24,42]. To avoid the over cure, the cure depth of acrylate-based material was studied in this work.

The cure depth of material was directly proportional to the exposure time and the standard cure depth of material for stereolithography presented by Jacobs's law [39]

$$C_d = D_p ln\left(\frac{I_{\max} T}{E_c}\right) \tag{2}$$

where C_d is the cure depth of material, $I_{\max}$ is the light intensity; T is the exposure time; E_c is the critical exposure of photocurable material, which is 0.80 J/cm^2 for transparent E-glass resin based on the experimental calculation; and D_p is the penetration depth of the exposure light. The polymerization of liquid resin is activated by the photo-initiator, and the light-absorbing dye can be applied to control the penetration depth of the projection light [42]. We conducted a series of curing experiments to adjust the cure depth of photocurable material, C_d by controlling the concentration of light-absorbing dye P_d and photo-initiaton P_I. Based on the experimental results, the concentration of photo-initiator P_I impacted the critical exposure E_c [41–43]. Meanwhile, after adding light-absorbing dye concentration P_d, the depth of light penetration in photopolymer was reduced. As a result, the cure depth of material C_d decreased along with the increase of light absorbing dye concentration P_d, and conversely, C_d increased with the increase of the concentration of photo-initiator, P_I. According to the Bear's law and Zissi's model [42–44], the cure depth of material C_d can be modulated by the below equation:

$$C_d = \frac{1}{\gamma P_d} ln\left(\frac{I_{\max} T (P_I)^{\frac{1}{2}}}{\alpha\beta}\right) l \tag{3}$$

where α and β is a constant for acrylate-based photochemical system, which is 1.38×10^{-5} and 9.06×10^{3} respectively for E-glass resin; γ is absorption coefficient of light absorber (317.46) when the concentrations of light-absorbing dye P_d and photo-initiator P_I are 0.5% and 1% , respectively. In ISA process, the photocurable polymer solution was developed with the values of P_I and P_d tuned for desired cure depth C_d in order to tightly attach the surface of the prebuilt object.

Process Planning of Hierarchical Three-Dimensional Printing. When the part is fabricated using a traditional single photopolymerization-based printing process, the digital model will be sliced into a set of 2D layers to generate the projection images or tool path [1]. Since the proposed hierarchical 3D

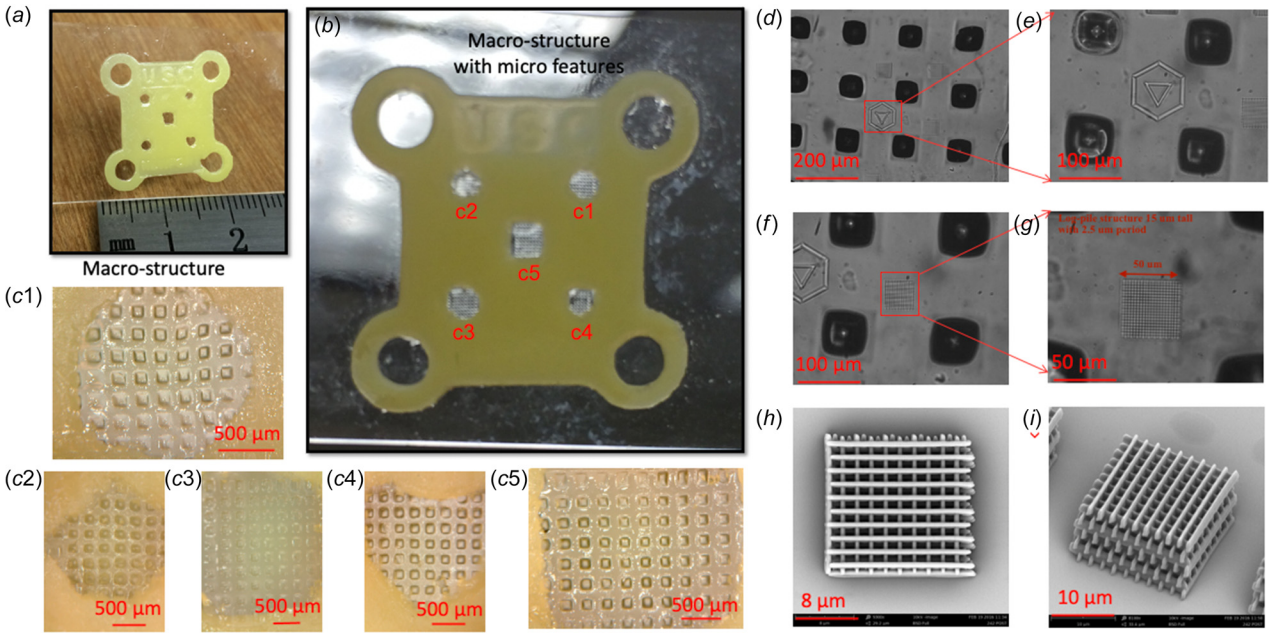

Fig. 5 A test case of macrostructures with micro-and nanofeatures: (*a*) macroscale structure built by the macroscale MIP-SL, (*b*) macro-and microscale structures built by the macroscale MIP-SL and the microscale ISA processes; (*c*1–*c*5) the microscope image of the microscale mesh matrix built by ISA in different-shaped holes, (*d*) the SEM image of the microscale mesh built by ISA with nanoscale structures built by TPP process, (*e*) the SEM image of the hexagon model fabricated by TPP with bigger magnifications, (*f*) the SEM image of a log-pile microstructure built by TPP on the top surface of the microscale mesh, (*g*) the SEM image of a log-pile microstructure built by TPP with bigger magnifications, and (*h*, *i*) the SEM images at different angle of a log-pile microstructure built by TPP

printing by integrating TPP, ISA, and MIP-SL can be controlled independently, separate geometry information at each scale was generated for the corresponding process. A sequential printing process coordinating macro-and meso scales 2D light beams and nanoscale laser beams with different printing resolutions was therefore developed. After being given an input 3D model, features, of which the cross-sectional area is bigger than 1 mm^2, were sliced to get the mask image and were further printed using the MIP-SL process. After that, microscale features with the area larger than 9×10^{-4} mm^2 were sliced and fabricated on the surface of prebuilt macroscale structures by using ISA. After the printing of macro-and microscales structures using MIP-SL and ISA, the printed object was fully cleaned using ethyl alcohol inside the ultrasonic bath for 30mins to remove the unpolymerized resin. Afterward, the printed object was thoroughly dried in a room environment to evaporate the remaining ethyl alcohol. Meanwhile, the submicron features were sliced into a set of voxels, of which the width d and height h were 500 nm and 500 nm, respectively. And then nanoscale features were printed in a voxel-by-voxel manner on the surface of the prebuilt microstructures. Finally, the cleaning of the final part after the printing of TPP was conducted. The sample was immersed in an ethanol bath for 20 min to wash away the residual liquid resin.

Experiment and Discussion

A mask planning testbed has been developed using the C++ language with the Microsoft Visual C++ compiler. The testbed integrated modules of geometry slicing, mask image generation, mask image projection, and motion controlling. To achieve multiscale fabrication, the testbed also synchronized the integration process based on the $X/Y/Z$ movements. In addition, a MATLAB program including imaging processing and object detecting was developed for the vision alignment in the ISA process. The testbed including 2D and 3D digital data import, coordinate transform, and motion control was developed based LABVIEW platform for the TPP process. Based on the proposed method, the fabricated results of two hierarchical structures by the integrated multiscale 3D printing process are shown in Figs. 5 and 6, respectively.

Multi-Scale Scaffold Fabrication. Figure 5 demonstrated a bioscaffold with multiscale structures. Fig. 5(*a*) shows the mesoscale structure printed by the MIP-SL process using resin SI500 (EnvisionTEC US LLC, Dearborn, MI). It contained five inner holes with different shapes (pentagon, circular, Hexagon, rectangle, and heart shape), of which the longest diameter was 2 mm, and the thickness of the printed mesoscale structure was 1 mm. Then the ISA process was used to print microscale scaffold mesh matrix in the same layer of the MIP printed mesoscale structure with biocompatible PEGDA solution (Fig. 5(*b*)). Each microhole fabricated by ISA was 100 μm in diameter as shown in Fig. 5(*c*). The PEGDA-based biocompatible hydrogel solution was made by 60 wt% PEGDA (Mw 700, purchased from Sigma-Aldirich, Envision TEC Inc., Dearborn, MI). The UV light photo-initiator (Irgacure 819, BASF) was used at a concentration of 1 wt% to induce chain polymerization by the free radicals. To prepare the resin, the photo-initiator was first fully dissolved in the phosphate buffered saline (PBS); we then added 60 wt% PEGDA into the PBS solution. To uniformly mix the solution, the magnetic stirrer was used for global agitation for 2 h and the mixture was put into the ultrasonic bath with a power of 700 W, frequency of 20 kHz, for 20 min.

Finally, two different shaped submicron structures were printed using the TPP. The SEM images of the micro- and nanoscales features fabricated by the TPP process are shown in Figs. 5(*d*)–5(*i*). Figs. 5(*d*) and 5(*e*) show the SEM images of the submicron hexagon line printed on the surface of the PEGDA microscale mesh matrix. Another 3D submicron log-pile structure printed by the TPP on the surface of the microscale mesh matrix built by the ISA is shown in Figs. 5(*f*) and 5(*g*). Figs. 5(*h*) and 5(*i*) show the top view and side view of the log-pile structure printed

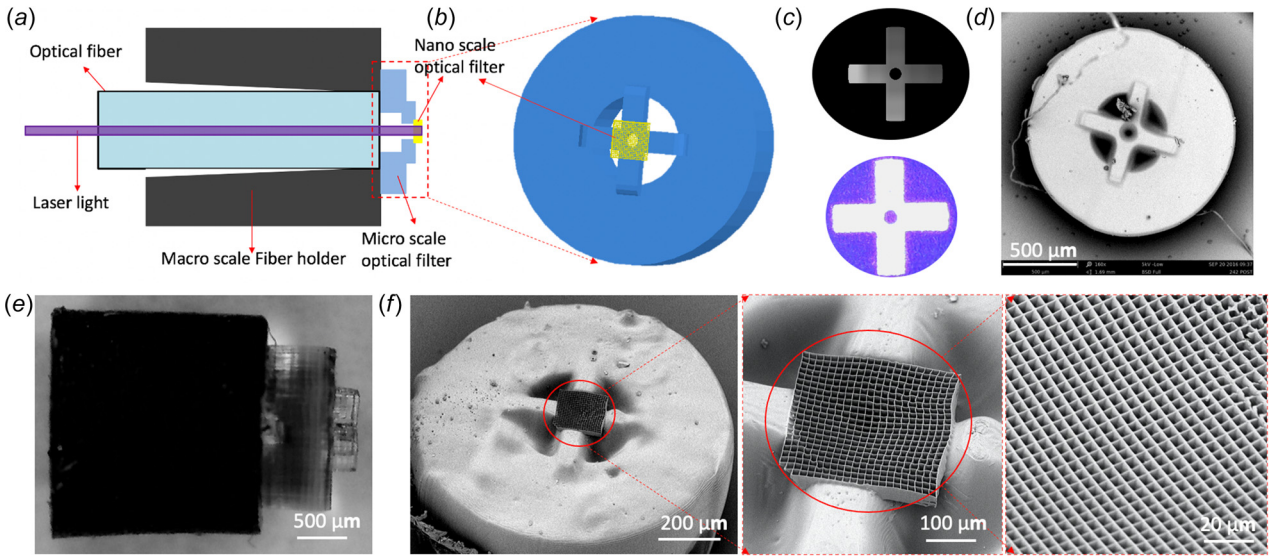

Fig. 6 The printing result of an optical filter with hierarchical structures ranging from macroscale to nanoscale: (*a*) the digital design of optical filter with hierarchical structures, (*b*) the microscale structure with nanoscale optical filter, (*c*) one layer of projection mask image and 2D patterned light beam used to fabricate the microscale optical filter support, (*d*) the SEM image of microscale optical filter support printed by microscale ISA process, (*e*) the macroscale optical fiber holder with microscale optical filter support, and (*f*) the SEM images of the submicron optical filter fabricated on the surface of microscale optical filter support using the nanoscale TPP process

by TPP. Such hierarchical multiscale structures have multiple potential applications for cell culture and drug screening [45,46].

Bio-Inspired Optical Filter. In nature, some creatures show the dazzling color that draws much attention. For example, butterfly's iridescent wings, fish's glaring scales, and peacock's colorful tail features [1]. These splendid colors are produced by the optical interaction of light with nanoscale structures [46–49]. Such structural color has inspired the innovations of artificial optical systems [47]. In this test, an optical filter with nanoscale structures whose dimension is close to the wavelength of light was designed. In addition, the macroscale assembly feature was designed with a tapper hole to enable the insert and removal of an optical fiber whose size is 800 μm (Fig. 6(*a*)). The optical device inspired by the butterfly hierarchical structure was successfully fabricated by the developed hierarchical printing method (Figs. 6(*d*)–6(*f*)).

The mesoscale optical fiber holder with the gradually decreasing microscale inner hole was fabricated by MIP-SL process with the E-Glass 3SP resin mixed with multiwall carbon nanotubes (MWCNTs). The total height of the cylindrical holder was 1.8 mm and the Z stage moved up 100 μm/layer to maintain the same thickness of the newly refilling material. The radiation of each pixel in the 2D patterned light beam implied a Gaussian intensity profile [23]. We applied a nonlinear exposure time set to maintain the printing accuracy by adjusting the exposure time based on exposure area. Consequently, the optimal exposure time of the first layer and the last layer was set as 15 s and 8 s, respectively, and the time for the interim layers was obtained through interpolation in a nonlinear manner. The desired tapered inner hole was successfully built without over-cured features which are caused by the energy accumulation, and the nonlinear exposure planning significantly enhanced the finishing quality of the part.

Specifically, the digital model of micro-and nanoscales optical filter is shown in Fig. 6(*b*). Using the 2D light beam projected from the calibrated mask image shown in Fig. 6(*c*), microscale filter support (Fig. 6(*d*)) was printed by ISA process with transparent E-Glass 3SP resin (EnvisionTEC Inc., Sigma Aldrich, St. Louis, MI) on the top surface of mesoscale optical fiber holder, which is designed with decreasing inner holes to ensure sufficient light going through during the TPP printing. As shown in Fig. 6(*e*), the microscale ISA processes were used to build the part and the layer thicknesses were set as 20 μm, respectively. The nanoscale features were built using a LABVIEW application capable of importing 2D and 3D digital files and transforming them into polyline coordinates, which will be read by the stacked XYZ stages used for the motion of the TPP process. The submicron optical filter was printed on the top surface of the hole of microscale filter support using acrylic-based resin (Fig. 6(*f*)).

Conclusions

The material systems in nature with exceptional performances benefit from hierarchical structures spanning over a large range of scales from macroscale to nanoscale. Such structures are usually associated with multiple scales of features with a large minimum to maximum ratio, which presents a significant challenge to existing manufacturing methods [2,9,49]. The aim of this research work is to investigate the integration of different photopolymerization-based AM processes ranging from macroscale to nanoscale to demonstrate the capability of fabricating multiscale functional material and hierarchical structures, in the hope to achieve numerous novel applications in different engineering fields. In this paper, a multiscale 3D printing process that integrates the macroscale MIP-SL, the microscale ISA, and the nanoscale TPP processes have been presented. The integration effort has been made for the fabrication of 3D objects with multiscale features. Taking advantage of the vision-assisted system, the sequential fabrication using the MIP-SL, ISA, and TPP systems can be integrated with satisfactory accuracy and resolution. Both hardware and software systems have been constructed to verify the developed multiscale fabrication approach. The experimental results based on two test cases demonstrated the effectiveness and feasibility of this integrated printing process in fabricating various multimaterial and multiscale hierarchical structures. This could open up novel hierarchical structure designs for various engineering fields in the future [50].

Acknowledgment

Authors acknowledge the Centre for Electron Microscopy and Micro-analysis (CEMMA) at USC for the use of microscopic measuring equipment.

Funding Data

- National Science Foundation (NSF) Division of Civil, Mechanical and Manufacturing Innovation (Grant Nos. 1151191 and 2114119; Funder ID: 10.13039/100000147).

Nomenclature

A = contact area
AM = additive manufacturing
C = the coordinates $C_0 \sim C_3$ of four corners of the region
C_d = cure depth of material
CCD = charge-coupled device
CMOS = complementary metal-oxide-semiconductor
D_p = penetration depth of the exposure light
DMD = digital micro-mirrors device
E_c = critical exposure of photocurable material
FDM = fused deposition modeling
I_{max} = maximum light intensity
ISA = immersed surface accumulation
LED = light-emitting diode
M = the coordinates of corners of the pre-built object
MIP-SL = mask image projection-based stereolithography
MWCNTs = multiwall carbon nanotubes
P = the coordinates of corners of the calibrated projection light beam
P_I = concentration of light photoinitiator
P_d = concentration of light absorber
PBS = phosphate buffered saline
PEGDA = poly(ethylene glycol) diacrylate
SEM = scanning electron microscope (SEM) image
SL = stereolithography
SLS/M = selective laser sintering /melting (SLS/M)
TPP = two-photon polymerization
UV = ultraviolet
T = exposure time
X' = corresponding distance in X direction
Y' = corresponding distance in X direction
2D = two-dimensional
3D = three-dimensional
γ = absorption coefficient of light absorber
σ_τ = the tensile stress of the material
$\alpha\beta$ = a constant for acrylate based photo-chemical system

References

[1] Wegst, U. G., Bai, H., Saiz, E., Tomsia, A. P., and Ritchie, R. O., 2015, "Bioinspired Structural Materials," Nat. Mater., **14**(1), pp. 23–36.
[2] Yang, Y., Song, X., Li, X., Chen, Z., Zhou, C., Zhou, Q., and Chen, Y., 2018, "Recent Progress in Biomimetic Additive Manufacturing Technology: From Materials to Functional Structures," Adv. Mater., **30**(36), p. e1706539.
[3] Liu, K., and Jiang, L., 2011, "Bio-Inspired Design of Multiscale Structures for Function Integration," Nano Today, **6**(2), pp. 155–175.
[4] Bhushan, B., 2009, "Biomimetics: Lessons From Nature–an Overview," Philos. Trans. R. Soc. A: Math., Phy. Eng. Sci., **367**(1893), pp. 1445–1486.
[5] Gu, G. X., Su, I., Sharma, S., Voros, J. L., Qin, Z., and Buehler, M. J., 2016, "Three-Dimensional-Printing of Bio-Inspired Composites," ASME J. Biomech. Eng, **138**(2), p. 21006.
[6] Kong, Y. L., Gupta, M. K., Johnson, B. N., and McAlpine, M. C., 2016, "3D Printed Bionic Nanodevices," Nano Today, **11**(3), pp. 330–350.
[7] Ke, P., Jiao, X. N., Ge, X. H., Xiao, W. M., and Yu, B., 2014, "From Macro to Micro: Structural Biomimetic Materials by Electrospinning," RSC Adv., **4**(75), pp. 39704–39724.
[8] Jonušauskas, L., Juodkazis, S., and Malinauskas, M., 2018, "Optical 3D Printing: Bridging the Gaps in the Mesoscale," J. Opt., **20**(5), p. 053001.
[9] Frazier, W. E., 2014, "Metal Additive Manufacturing: A Review," J. Mater. Eng. Perform., **23**(6), pp. 1917–1928.
[10] Leung, Y. S., Kwok, T. H., Li, X., Yang, Y., Wang, C. C., and Chen, Y., 2019, "Challenges and Status on Design and Computation for Emerging Additive Manufacturing Technologies," ASME J. Comput. Inf. Sci. Eng., **19**(2), p. 021013.
[11] Kolesky, D. B., Truby, R. L., Gladman, A. S., Busbee, T. A., Homan, K. A., and Lewis, J. A., 2014, "3D Bioprinting of Vascularized, Heterogeneous Cell-Laden Tissue Constructs," Adv. Mater., **26**(19), pp. 3124–3130.
[12] Au, A. K., Huynh, W., Horowitz, L. F., and Folch, A., 2016, "3D-Printed Microfluidics," Angew. Chem. Int. Ed., **55**(12), pp. 3862–3881.
[13] Wu, W., DeConinck, A., and Lewis, J. A., 2011, "Omnidirectional Printing of 3D Microvascular Networks," Adv. Mater., **23**(24), pp. H178–H183.
[14] Li, Y., Mao, H., Hu, P., Hermes, M., Lim, H., Yoon, J., Luhar, M., Chen, Y., and Wu, W., 2019, " Bioinspired Functional Surfaces Enabled by Multiscale Stereolithography," Adv. Mater. Tech., **4**(5), p. 1800638.
[15] Mao, H., Leung, Y. S., Li, Y., Hu, P., Wu, W., and Chen, Y., 2017, "Multiscale Stereolithography Using Shaped Beams," ASME J. Micro Nano-Manuf., **5**(4), p. 40905.
[16] Zhou, C., Ye, H., and Zhang, F., 2015, "A Novel Low-Cost Stereolithography Process Based on Vector Scanning and Mask Projection for High-Accuracy, High-Speed, High-Throughput, and Large-Area Fabrication," ASME J. Comput. Inf. Sci. Eng., **15**(1), p. 011003.
[17] Jia, W., Leung, Y. S., Mao, H., Xu, H., Zhou, C., and Chen, Y., 2022, "Hybrid-Light-Source Stereolithography for Fabricating Macro-Objects With Micro-Textures," ASME J. Manuf. Sci. Eng., **144**(3), p. 031003.
[18] Porter, B. F., Mkhize, N., and Bhaskaran, H., 2017, "Nanoparticle Assembly Enabled by EHD-Printed Monolayers," Microsyst. Nanoeng., **3**(1), pp. 1–9.
[19] Choi, J. W., Yamashita, M., Sakakibara, J., Kaji, Y., Oshika, T., and Wicker, R. B., 2010, "Combined Micro and Macro Additive Manufacturing of a Swirling Flow Coaxial Phacoemulsifier Sleeve With Internal Micro-Vanes," Biomed. Microdev., **12**(5), pp. 875–886.
[20] Hengsbach, S., and Lantada, A. D., 2014, " Rapid Prototyping of Multi-Scale Biomedical Microdevices by Combining Additive Manufacturing Technologies," Biomed. Microdev., **16**(4), pp. 617–627.
[21] Malinauskas, M., Rekštytė, S., Lukoševičius, L., Butkus, S., Balčiūnas, E., Pečiukaitytė, M., Baltriukienė, D., Bukelskienė, V., Butkevičius, A., Kucevičius, P., Rutkūnas, V., and Juodkazis, S., 2014, "3D Microporous Scaffolds Manufactured Via Combination of Fused Filament Fabrication and Direct Laser Writing Ablation," Micromachines, **5**(4), pp. 839–858.
[22] Autumn, K., and Gravish, N., 2008, "Gecko Adhesion: Evolutionary Nanotechnology," Philos. Trans. R. Soc. London, Ser A: Math., Phy. Eng. Sci., **366**(1870), pp. 1575–1590.
[23] Zhou, C., Chen, Y., and Waltz, R. A., 2009, "Optimized Mask Image Projection for Solid Freeform Fabrication," ASME J. Manuf. Sci. Eng., **131**(6), p. 61004.
[24] Zhou, C., and Chen, Y., 2012, "Additive Manufacturing Based on Optimized Mask Video Projection for Improved Accuracy and Resolution," J. Manuf. Processes, **14**(2), pp. 107–118.
[25] Li, X., Mao, H., Pan, Y., and Chen, Y., 2019, "Mask Video Projection-Based Stereolithography With Continuous Resin Flow," ASME J. Manuf. Sci. Eng., **141**(8), p. 81007.
[26] Pan, Y., Zhou, C., and Chen, Y., 2012, "A Fast Mask Projection Stereolithography Process for Fabricating Digital Models in Minutes," ASME J. Manuf. Sci. Eng., **134**(5), p. 51011.
[27] Zhou, C., Chen, Y., Yang, Z., and Khoshnevis, B., 2013, "Digital Material Fabrication Using Mask-Image-Projection-Based Stereolithography," Rapid Prototyping J., **19**(3), pp. 153–165.
[28] Pan, Y., Chen, Y., and Yu, Z., 2017, "Fast Mask Image Projection-Based Micro-Stereolithography Process for Complex Geometry," ASME J. Micro/Nano-Manuf., **5**(1), p. 014501.
[29] Li, X., Yang, Y., Xie, B., Chu, M., Sun, H., Hao, S., Chen, Y., and Chen, Y., 2019, "3D Printing of Flexible Liquid Sensor Based on Swelling Behavior of Hydrogel With Carbon Nanotubes," Adv. Mater. Tech., **4**(2), p. 1800476.
[30] Li, X., Xie, B., Jin, J., Chai, Y., and Chen, Y., 2018, "3D Printing Temporary Crown and Bridge by Temperature Controlled Mask Image Projection Stereolithography," Procedia Manuf., **26**, pp. 1023–1033.
[31] Yang, Y., Li, X., Chu, M., Sun, H., Jin, J., Yu, K., Wang, Q., Zhou, Q., and Chen, Y., 2019, "Electrically Assisted 3D Printing of Nacre-Inspired Structures With Self-Sensing Capability," Sci. Adv., **5**(4), p. eaau9490.
[32] Wu, E. S., Strickler, J. H., Harrell, W. R., and Webb, W. W., 1992, "Two-Photon Lithography for Microelectronic Application," Proc. Opt./Laser Microlith. V, **1674**, pp. 776–782.
[33] Maruo, S., Nakamura, O., and Kawata, S., 1997, "Three-Dimensional Microfabrication With Two-Photon-Absorbed Photopolymerization," Opt. Lett., **22**(2), pp. 132–134.
[34] Cheng, J., Gu, C., Zhang, D., Wang, D., and Chen, S. C., 2016, "Ultrafast Axial Scanning for Two-Photon Microscopy Via a Digital Micromirror Device and Binary Holography," Opt. Lett., **41**(7), pp. 1451–1454.
[35] Jiang, L., Xiong, W., Zhou, Y., Liu, Y., Huang, X., Li, D., Baldacchini, T., Jiang, L., and Lu, Y., 2016, "Performance Comparison of Acrylic and Thiol-Acrylic Resins in Two-Photon Polymerization," Opt. Express, **24**(12), pp. 13687–13701.
[36] Baldacchini, T. (Ed.)., 2015, *Three-Dimensional Microfabrication Using Two-Photon Polymerization: Fundamentals, Technology, and Applications*, Chapter 1–3, William Andrew, New York.
[37] Li, X., and Chen, Y., 2017, "Micro-Scale Feature Fabrication Using Immersed Surface Accumulation," J. Manuf. Processes, **28**(3), pp. 531–540.
[38] Yang, Y., Li, X., Zheng, X., Chen, Z., Zhou, Q., and Chen, Y., 2018, "3D-Printed Biomimetic Super-Hydrophobic Structure for Microdroplet Manipulation and Oil/Water Separation," Adv. Mater., **30**(9), p. 1704912.
[39] Li, X., Yang, Y., Liu, L., Chen, Y., Chu, M., Sun, H., Shan, W., and Chen, Y., 2020, "3D-Printed Cactus-Inspired Spine Structures for Highly Efficient Water Collection," Adv. Mater. Interfaces, **7**(3), p. 1901752.
[40] Hribar, K. C., Finlay, D., Ma, X., Qu, X., Ondeck, M. G., Chung, P. H., Zanella, A., Engler, A. J., Sheikh, F., Vuori, K., and Chen, S. C., 2015, "Nonlinear 3D Projection Printing of Concave Hydrogel Microstructures for Long-Term

Multicellular Spheroid and Embryoid Body Culture," Lab a Chip, **15**(11), pp. 2412–2418.
[41] Jacobs, P. F., 1992, *Rapid Prototyping & Manufacturing: Fundamentals of Stereolithography*, Society of Manufacturing Engineers, Southfield, MI.
[42] Jacobs, P. F., 1995, *Stereolithography and Other RP&M Technologies: From Rapid Prototyping to Rapid Tooling*, Society of Manufacturing Engineers, Southfield, MI.
[43] Lee, J. H., Prud'Homme, R. K., and Aksay, I. A., 2001, "Cure Depth in Photopolymerization: Experiments and Theory," J. Mater. Res., **16**(12), pp. 3536–3544.
[44] Gong, H., Beauchamp, M., Perry, S., Woolley, A. T., and Nordin, G. P., 2015, "Optical Approach to Resin Formulation for 3D Printed Microfluidics," RSC Adv., **5**(129), pp. 106621–106632.
[45] Zissi, S., Bertsch, A., Jézéquel, J. Y., Corbel, S., Lougnot, D. J., and Andre, J. C., 1996, "Stereolithography and Microtechniques," Microsyst. Technol., **2**(2), pp. 97–102.
[46] Zhu, Y., Joralmon, D., Shan, W., Chen, Y., Rong, J., Zhao, H., Xiao, S., and Li, X., 2021, "3D Printing Biomimetic Materials and Structures for Biomedical Applications," Bio-Des. Manuf., **4**(2), pp. 405–28.
[47] Zhao, Y., Xie, Z., Gu, H., Zhu, C., and Gu, Z., 2012, "Bio-Inspired Variable Structural Color Materials," Chem. Soc. Rev., **41**(8), pp. 3297–3317.
[48] Kim, S., Shin, J. H., Kim, S., Yoo, S. J., Jun, B. O., Moon, C., and Jang, J. E., 2016, "Geometric Effects of Nano-Hole Arrays for Label Free Bio-Detection," RSC Adv., **6**(11), pp. 8935–8940.
[49] Zhang, W., Zhang, D., Fan, T., Gu, J., Ding, J., Wang, H., Guo, Q., and Ogawa, H., 2009, "Novel Photoanode Structure Templated From Butterfly Wing Scales," Chem. Mater., **21**(1), pp. 33–40.
[50] Zhu, Y., Tang, T., Zhao, S., Joralmon, D., Poit, Z., Ahire, B., Keshav, S., Raje, A. R., Blair, J., Zhang, Z., and Li, X., 2022, "Recent Advancements and Applications in 3D Printing of Functional Optics," Addit. Manuf., **52**, p. 102682.